



Residual eccentricity as a systematic uncertainty on the formation channels of binary black holes

Giulia Fumagalli ^{1,2,*} Isobel Romero-Shaw ^{3,4} Davide Gerosa ^{1,2}
Viola De Renzi ^{1,2} Konstantinos Kritos ⁵ and Aleksandra Olejak ⁶

¹*Dipartimento di Fisica “G. Occhialini”, Università degli Studi di Milano-Bicocca, Piazza della Scienza 3, 20126 Milano, Italy*

²*INFN, Sezione di Milano-Bicocca, Piazza della Scienza 3, 20126 Milano, Italy*

³*Department of Applied Mathematics and Theoretical Physics, Cambridge CB3 0WA, United Kingdom*

⁴*Kavli Institute for Cosmology Cambridge, Madingley Road Cambridge CB3 0HA, United Kingdom*

⁵*William H. Miller III Department of Physics and Astronomy,
Johns Hopkins University, Baltimore, Maryland 21218, USA*

⁶*Max Planck Institut für Astrophysik, Karl-Schwarzschild-Straße 1, 85748 Garching bei München, Germany*

(Dated: May 27, 2024)

Resolving the formation channel(s) of merging binary black holes is a key goal in gravitational-wave astronomy. The orbital eccentricity is believed to be a precious tracer of the underlying formation pathway, but is largely dissipated during the usually long inspiral between black-hole formation and merger. Most gravitational-wave sources are thus expected to enter the sensitivity windows of current detectors on configurations that are compatible with quasi-circular orbits. In this paper, we investigate the impact of “negligible” residual eccentricity—lower than currently detectable by LIGO/Virgo—on our ability to infer the formation history of binary black holes, focusing in particular on their spin orientations. We trace the evolution of both observed and synthetic gravitational-wave events backward in time, while resampling their residual eccentricities to values that are below the detectability threshold. Eccentricities in-band as low as $\sim 10^{-4}$ can lead to significant biases when reconstructing the spin directions, especially in the case of loud, highly precessing systems. Residual eccentricity thus act like a systematic uncertainty for our astrophysical inference. As a mitigation strategy, one can marginalize the posterior distribution over the residual eccentricity using astrophysical predictions.

I. INTRODUCTION

Inferring the formation and evolutionary processes of merging stellar-mass black holes (BHs) is one of the most pressing questions in modern high-energy astrophysics. LIGO and Virgo are delivering hundreds of gravitational-wave (GW) detections [1–4] and, despite some initial optimism, the “formation-channel” problem is still far from solved [5–10]. BHs are simple objects in General Relativity, which implies we have a limited number of observables at our disposal, notably masses, spins, merger rates, and potentially the orbital eccentricity. Among these, spin directions [11–18] and eccentricity [19–21] are believed to be clean indicators of the BH progenitors and their formation mechanisms, with large spin misalignments and large eccentricities pointing to dynamical assembly in newdensely populated environments.

Spin precession and orbital eccentricity are deeply intertwined. From a signal perspective, they both introduce on timescales that are longer than that of the orbit [22–24]. Such waveform features can be comparable, and isolating the two effects in current GW data presents challenges, at least for sufficiently short signals [25]. As for the binary evolution, couplings between the spin and eccentricity sectors of the binary dynamics introduces a non-trivial phenomenology. Sources formed with identical

parameters but different eccentricities might enter the LIGO/Virgo band with spin evolution patterns that are considerably different [26].

This interplay between spins and eccentricity requires careful consideration when reconstructing the history of BH binaries from their parameters, which are inferred from their GW signals. Propagating spin directions from formation to detection [27, 28] is crucial to transfer astrophysical predictions to the regime where sources are observable [11, 12, 15], thus allowing for a meaningful comparison with the data. The reverse operation, “back-propagating” binaries from detection to formation, has key applications in single-event inference [29–31], population studies [29, 32], and archival searches for, say, the LISA mission [33–36]. In this paper, we show that eccentricity is a source of systematics that might affect, perhaps significantly, these downstream applications.

The BH binaries observed by LIGO and Virgo have been consistently reported to be quasi-circular [37, 38], perhaps with a few exceptions [39, 40]. This is not surprising, as leading-order post-Newtonian (PN) effects tend to remove eccentricity from binary systems on a timescale that is shorter than that of the inspiral itself [41], leading to quasi-circular mergers even for systems that initially formed on highly eccentric orbits. Current ground-based interferometers are capable of detecting eccentricities as low as $e_{\text{thr}} \simeq 0.05$ for GW150914-like binaries [42], meaning that binaries entering the sensitivity band of our instruments with eccentricities lower than this threshold will be reported as quasi-circular. In reality, GW sources

* g.fumagalli47@campus.unimib.it

have some residual eccentricity $e_{\text{res}} < e_{\text{thr}}$ which cannot be captured. For typical astrophysical environments, current models predict values of $e_{\text{res}} \lesssim 10^{-8}$ for field binaries and $\sim 10^{-7} \lesssim e_{\text{res}} \lesssim 10^{-4}$ for the majority of binaries formed in clusters (cf. Sec. III C below). For binaries that are assembled dynamically, models also predict a small fraction of sources merging with $e_{\text{res}} > e_{\text{thr}}$ which, if detected, are poised to be highly informative [20].

Quasi-circular orbits act as dynamical attractors for the forward evolution of BH binaries [41], which unfortunately implies they act as repulsor where sources are back-propagated: for binaries on eccentric orbits, small variations of their parameters at GW detection implies large variations at BH formation. As first identified in previous work by some of us [26], this issue is particularly concerning when considering the spin directions. Do residual, below-threshold eccentricities significantly affect our inference on the spin of BH binaries and thus their formation mechanism? How can this source of systematic be mitigated? What are the consequences when inferring the formation channels of GW sources?

We tackle these questions by applying the PN formalism of Refs. [26, 28] to real LIGO/Virgo observations, synthetic GW events, and predictions from astrophysical population-synthesis simulations. For each event, instead of making the common assumption that $e_{\text{res}} = 0$, we resample the residual eccentricity $e_{\text{res}} < e_{\text{thr}}$ and back-propagate the resulting spin evolution to a common large separation. We compare the resulting spin distributions against those obtained assuming quasi-circularity for the entire inspiral.

For current events up to GWTC-3 [1–4], we find that residual eccentricity introduces a rather mild systematic effect. This is due to the large uncertainties on the spin directions as well as the weak or absent evidence of spin precession in most of the signals. We are safe, for now. Using a set of synthetic injections [43] with higher signal-to-noise ratios (SNR) and prominent two-spin effects, we observe severe divergences between the eccentric and quasi-circular spin predictions. Unaccounted (and, at present, unaccountable) eccentricity at detection can introduce substantial variation in our inference of spins at BH binary formation, which implies that residual eccentricity is effectively a systematic one should take into account when inferring the origin of GW events. We show that astrophysical models of BH binary formation [44–46] can be used to heuristically “marginalize” over this systematic, thereby mitigating its impact.

Our paper is organized as follows: in Sec. II we summarize the back-propagation procedure, the adopted statistical tools, and the targeted GW events; in Sec. III we present our results in terms of the bias induced and propose a strategy to marginalize over residual eccentricity using astrophysical predictions; in Sec. IV we discuss the implications of our findings.

II. BACK PROPAGATION

A. Black-hole binary dynamics

BH binaries are characterized by masses $m_{1,2}$, mass ratio $q = m_2/m_1 \leq 1$, total mass $M = m_1 + m_2$, dimensionless spin magnitudes $\chi_{1,2} \in [0, 1]$, polar spin angles $\theta_{1,2} \in [0, \pi]$ measured from the orbital angular momentum, and azimuthal spin angles $\Phi_{1,2}$ measured in the orbital plane. As long as the orbital timescale is much shorter than the inspiral timescale, orbits can be described using Keplerian notions for the semi-major axis a and the orbital eccentricity $e \in [0, 1)$. Hereafter we set $c = G = 1$.

Spin information is often condensed into the parameters χ_{eff} (which includes information about the aligned components of the spins [47]) and χ_{p} (which instead captures spin precession [48, 49]). In the following, we use the “average” definition of χ_{p} put forward in Refs. [43, 49]. In particular, one has $\chi_{\text{p}} \in [0, 2]$ where the lower bound implies aligned spins and $\chi_{\text{p}} > 1$ implies that both spins are precessing. Such definition can be trivially extended to eccentric orbits using the mapping detailed in Ref. [26]. In particular it is sufficient to substitute $r \rightarrow a(1 - e^2)$ in the calculations of Ref. [49].

We evolve binaries along their inspiral using the precession-averaged PN approach of Refs. [26, 28]; we refer to those previous papers for extensive derivation and validation of the formalism. In brief, we first neglect radiation reaction and solve the spin-precession problem semi-analytically by exploiting constants of motion [47, 50]. GW emission is then introduced quasi-adiabatically, modeling the spin evolution as a continuous series of those semi-analytic solutions. Initially restricted to circular sources [27, 28], precession-averaged PN evolutions have been recently extended to small-to-moderate eccentricities $e \lesssim 0.6$ [26], where the limitation is set by the validity of the underlying orbit-averaged PN equations [41].

Posterior samples are provided at the reference GW frequency $f_{\text{ref}} = 20$ Hz, with the exception of GW190521 where instead $f_{\text{ref}} = 11$ Hz [2]. From these, we calculate the semi-major axis a using the PN expression reported in Eq. (4.13) of Ref. [23], which results in separations of $\mathcal{O}(10M)$. This conversion neglects the presence of eccentricity, which is appropriate for $e_{\text{res}} < e_{\text{thr}}$.

B. Residual eccentricity

Residual eccentricity in-band might go unnoticed. We capture this effect by assigning each posterior sample a new value of the eccentricity that is below distinguishability threshold. In the following, we pursue two strategies:

- (i) For a rather agnostic approach, we consider thermal distributions $f(e) \propto e$ which naturally arise in statistical physics. We set $e \in [0, e_{\text{max}}]$ such that $e_{\text{max}} = 0$ corresponds to assuming binaries that evolved on quasi-circular orbits since formation. In the follow-

ing, we use $e_{\max} = 10^{-4}, 10^{-3}, 10^{-2}$ such that all samples have an eccentricity $e \leq e_{\max} < e_{\text{thr}} \simeq 0.05$ in band. Note that eccentricities are resampled at $f_{\text{ref}} = 20, 11$ Hz while Ref. [42] quotes the threshold $e_{\text{thr}} \sim 0.05$ at 10 Hz. We check that our resampled values of e_{res} are lower than e_{thr} : using Peters' equations [41], a binary $e = 10^{-2}$ at 20 Hz reaches $e \sim 0.02$ at 10 Hz. For a more in-depth study, one should consider an eccentricity threshold that depends on the binary parameters (for instance: it is easier to infer the eccentricity for binaries with lower masses because they complete more cycles in band [51]). We leave this to future work.

- (ii) For a more astrophysical motivated approach, we attempt a direct modeling of the residual eccentricity predicted by state-of-the-art population-synthesis codes. We make use of simulations of both binaries formed in isolation [52] and binaries assembled dynamically in dense stellar clusters [21, 46]. We draw eccentricities directly from their distributions as predicted at GW detection; see Sec. III C for details. In particular, distributions are truncated at $e_{\text{res}} < e_{\text{thr}}$. This mimics a scenario where highly eccentric sources predicted can be identified as such and are not affected by the systematic uncertainty targeted here.

Given this initial configuration, we propagate binaries backward in time until the separation reaches $a = 10^4 M$. This is rather conservative as BH binary formation typically happens as separations as large as $\sim 10^6 M$ [46, 53, 54]. If the residual eccentricity in band is $\neq 0$, binaries will reach this large separation with orbits that are considerably more eccentric; this is due to the repulsive character of Peters' [41] equations. When back propagating from eccentricities e_{res} of $\mathcal{O}(10^{-2})$, the resulting eccentricities at $a = 10^4 M$ can be larger than 0.6, which was quoted as a conservative limit for validity of our formalism [26]. Extending the applicability of PN integrations in the high-eccentricity regime is conceptual problem which is outside of the scope of this paper. For simplicity, here we nonetheless use the Peters' equations for all our sources, which is in line with common practice in the astrophysical community.

C. Gravitational-wave signals

We consider both current LIGO/Virgo observations as well as synthetic injections. Together, these sources cover a broad range of SNRs and degrees of spin precession.

- (i) We consider 69 binary BH mergers as reported in the currently available GWTC catalog[1–4], selecting events with false alarm rate $< 1 \text{ yr}^{-1}$ and astrophysical probability $p_{\text{astro}} > 0.5$. We use samples labeled as Mixed-Cosmo which combine results

from the IMRPHEenomXPHM [55] and SEOB-NRv4PHM [56] waveform approximants. For event GW200129_065458 we also consider posterior samples obtained with NRSUR7DQ4 [57] from Ref. [58], which present a much stronger evidence for spin precession (see also Ref. [59] for similar conclusions and Ref. [60] for caveats related to data quality).

- (ii) We also use 100 publicly available [61] software injections which specifically target highly precessing systems. These were first presented in Figs. 4 and 5 of Ref. [43]. The parameters of these sources are distributed by reweighting the uninformative prior used in LIGO/Virgo parameter estimation in favor of a uniform distribution in $\chi_p \in [0, 2]$ and applying a SNR threshold of 20. In particular, these binaries have masses $m_{1,2} \in [5, 100] M_{\odot}$ constrained to $q \in [1/8, 1]$ and $\mathcal{M}_c \in [10, 60] M_{\odot}$ (where \mathcal{M}_c is the detector-frame chirp mass), spins $\chi_{1,2} \in [0, 0.99]$, and luminosity distances $D_L \in [100, 5000]$ Mpc. Source are injected and recovered with the IMRPHEenomXPHM [55] approximant, assuming detector performances representative of the 4th observing run of LIGO/Virgo and neglecting non-stationary noise realizations (for details see Ref. [43]).

Crucially, all these sources, both real and synthetic, have been analyzed assuming BHs on quasi-circular orbits. We do not have posterior distributions for the residual eccentricity in band, which thus acts as a systematic uncertainty.

D. Hellinger distance

Quantifying the impact of residual eccentricities requires a notion of distance between probability distributions. Among the many available options [62], we opt for the Hellinger distance [63]. This is defined as

$$d_{\text{H}}(p, q) = \sqrt{1 - \int \sqrt{p(x)q(x)} dx}, \quad (1)$$

where p and q are probability density functions of a (possibly multi-dimensional) variable x . In our case, these are the back-propagated posteriors obtained assuming either quasi-circularity or resampled eccentricities, respectively. We integrate over $x = (\cos \theta_1, \cos \theta_2)$ and have verified that $x = \chi_p$ yields results that are largely indistinguishable. We evaluate probability density functions using Kernel Density Estimation and compute the integral in Eq. (1) via Monte Carlo.

The Hellinger distance has the desirable properties of being symmetric, i.e. $d_{\text{H}}(p, q) = d_{\text{H}}(q, p)$, and defined in $[0, 1]$ such that $d_{\text{H}} = 0$ implies that the two distributions are identical and $d_{\text{H}} = 1$ implies that their supports are disjoint. For some intuition, one can convert Hellinger-distance values into σ levels by considering two

	1σ	2σ	3σ	4σ	5σ	\dots	10σ
d_{H}	0.343	0.627	0.822	0.930	0.978	\dots	$\sim 1-10^{-6}$

TABLE I. Values of the Hellinger distance for two identical Gaussian distributions separated by an increasing number n of standard deviations σ .

one-dimensional Gaussians separated by n standard deviations. The results is

$$d_{\text{H}}[\mathcal{N}(\mu, \sigma), \mathcal{N}(\mu + n\sigma, \sigma)] = \sqrt{1 - \exp\left(-\frac{n^2}{8}\right)}. \quad (2)$$

Some evaluations are reported in Table I.

III. SYSTEMATIC UNCERTAINTY

A. A few examples

The top panels of Fig. 1 show posterior distributions of the spin angles (θ_1, θ_2) and the effective precession parameter χ_{p} for the synthetic event labeled as `uni_88` in the dataset of Ref. [61]. This signal was handpicked for illustrative purposes because it has the largest Hellinger distance between the quasi-circular and eccentric reconstructions. This is a loud (SNR $\simeq 118$) system with BHs of detector-frame masses $m_1 = 49.5_{-1.8}^{+1.2} M_{\odot}$, $m_2 = 45.3_{-1.1}^{+1.1} M_{\odot}$ and spin magnitudes $\chi_1 = 0.95_{-0.06}^{+0.03}$, $\chi_2 = 0.94_{-0.07}^{+0.04}$ (hereafter we report medians and 90% credible intervals). We show posterior distributions at detection ($f_{\text{ref}} = 20$ Hz) as well as those resulting from our back-propagation procedure ($a = 10^4 M$) assuming residual eccentricities extracted from a thermal distribution truncated at some e_{max} .

As the adopted residual eccentricity increases, the back-propagated posterior distributions show larger deviations from the expected circular predictions, possibly leading to biased estimations of the spin parameters. For this event, the Hellinger distance between the back-propagated posterior obtained with $e_{\text{max}} = 10^{-2}$ and its circular counterpart with $e_{\text{max}} = 0$ is ~ 0.79 (i.e. $\gtrsim 2\sigma$ levels).

It is informative to compare the locations of the back-propagated distributions against those at detection as a function of the residual eccentricity. When projected in the $(\cos\theta_1, \cos\theta_2)$ plane, all distributions lie roughly on the same diagonal line; this is because χ_{eff} is a constant of motion for both the eccentric and the quasi-circular problem [47] (at least at 2PN in spin precession, which is the order considered here). But crucially, larger residual eccentricities imply spin orientations that are closer to those at detection.

While this might seem counterintuitive at first, it is a direct consequence of the PN equations of motion [26, 64]. The evolution of the spin orientations depends on semi-major axis a and eccentricity e through the orbital angular momentum L . This acts much like a time coordinate, with sources evolving from large L to small L .

From the Newtonian scaling $L \propto \sqrt{a(1-e)}$, eccentric binaries have a smaller angular momentum than circular binaries for a given value of a . The posteriors shown in Fig. 1 are naturally ordered by angular momentum, with the eccentric back-propagated posteriors seated between the back-propagated circular posteriors (which have the largest orbital angular momentum) and the posteriors at detection (which have the smallest orbital angular momentum).

The bottom panels of Fig. 1 show back-propagated posteriors for the LIGO/Virgo event GW191109_010717; once more, this system was chosen for its most pronounced differences between eccentric and circular back-propagated results across the current GW catalog. GW191109_010717 has an SNR of ~ 13.6 and is consistent with a binary BH with $m_1 = 81_{-9}^{+13} M_{\odot}$, $m_2 = 60_{-17}^{+16} M_{\odot}$, $\chi_1 = 0.65_{-0.58}^{+0.32}$, and $\chi_2 = 0.82_{-0.57}^{+0.15}$. Although subtler, the same features we discussed for our simulated system are also present for GW191109_010717; this is, however, characterized by much larger uncertainties (the SNR is about 10 times lower). In this case, we report a distance $d_{\text{H}} \sim 0.01$ between back-propagated posteriors with $e_{\text{max}} = 10^{-2}$ and $e_{\text{max}} = 0$. Overall, this shows that, for current events, the systematic bias induced by neglecting residual eccentricity in band is mild. It might, however, become important for exceptionally loud events and/or with the next leap in sensitivity of our detectors. Despite the promising evidence for precession in GW200129_065458 [58, 59], we find $d_{\text{H}} \sim 10^{-5}$ between back-propagated posteriors with $e_{\text{max}} = 10^{-2}$ and $e_{\text{max}} = 0$ when using the samples of Ref. [58]. This is likely attributed to the largely unconstrained posterior for the secondary spin.

B. Parameter-space exploration

We now present a broader exploration of the parameter space using the Hellinger distance (Sec. IID) as our summary statistic. Figure 2 shows the values of d_{H} across our two datasets of real and simulated events, cf. Sec. IIC. We compute Hellinger distances between the three eccentric back-propagated distributions $e_{\text{max}} = 10^{-2}, 10^{-3}, 10^{-4}$ and the circular case $e_{\text{res}} = e_{\text{max}} = 0$. The distance is computed over $x = (\cos\theta_1, \cos\theta_2)$ and plotted against the median value of χ_{p} at detection.

The Hellinger distance between our circular and eccentric back-propagated prediction increases with χ_{p} , indicating that the systematic uncertainty associated with residual eccentricity is strongly correlated with the amount of precession in the signal. More trivially and as already illustrated in Fig. 1, we find that the distance increases with e_{max} .

On top of these main trends, Fig. 2 shows substantial variability, even across several orders of magnitude in d_{H} . This is not surprising given the high dimensionality of the BH binary parameter space and our sparse coverage. For a given value of χ_{p} and e_{max} , we find that sources at lower

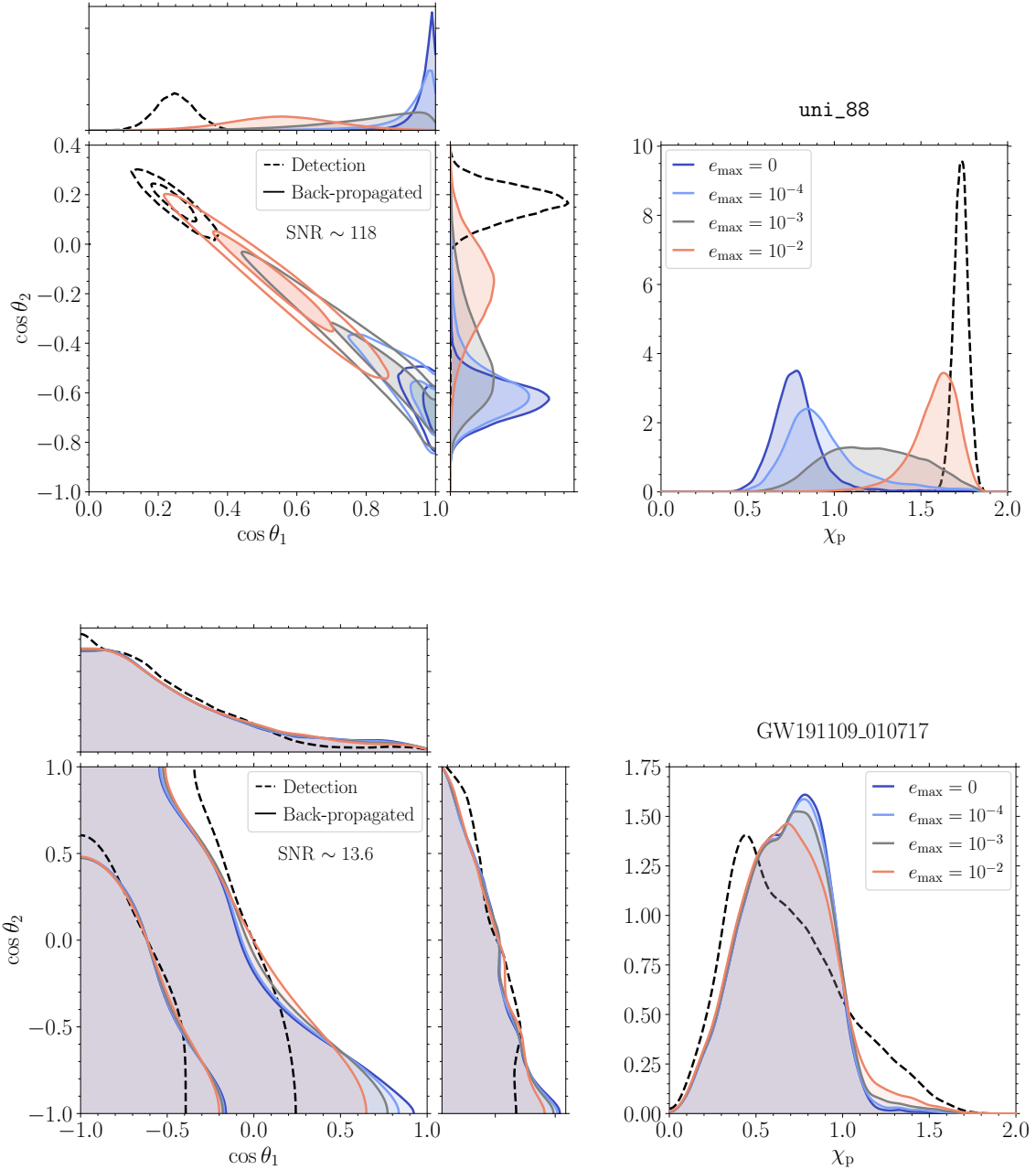


FIG. 1. Back-propagated posterior distributions assuming both eccentric and quasi-circular configurations. The top panels show results for the synthetic signal labeled **uni_88** in the dataset of Ref. [61]; the bottom panel shows event event GW191109_010717 [4]. In both cases, left panels shows the joint posterior distribution of the spin orientations (θ_1, θ_2) and right panels shows the posterior distribution of χ_p . Dashed curves show the distributions at detection ($f_{\text{ref}} = 20$ Hz); solid curves are obtained by back-propagating posterior samples to $a = 10^4 M$. The dark blue distributions ($e_{\text{max}} = 0$) assumes sources evolved on quasi-circular orbit throughout their inspiral. The other curves assume some residual eccentricity at detection. These are drawn from a thermal distribution $f(e) \propto e$ truncated at $e_{\text{max}} = 10^{-4}$ (light blue), 10^{-3} (gray), and 10^{-2} (red). Contours in the 2-dimensional distributions on the left correspond to 50% and 90% credible intervals. An animated version of this figure is available at www.davidegerosa.com/spinprecession.

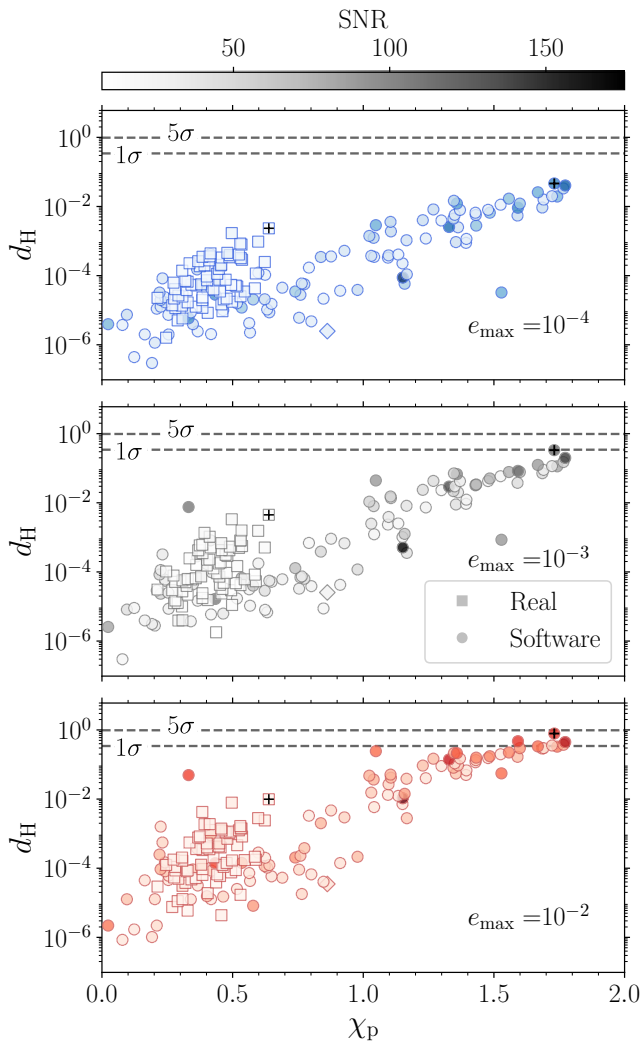


FIG. 2. Hellinger distances between circular and eccentric back-propagated posterior distributions of $(\cos \theta_1, \cos \theta_2)$ as a function of the median value of χ_p at detection. We consider 69 real events detected by LIGO/Virgo (squares) and 100 synthetic signals (circles). Diamonds mark results obtained using the posteriors samples of Ref. [58] for event GW200129_065458. Crosses indicate the events used in Figs. 1 and 4. Panels and colors refer to different assumptions for the residual eccentricity in band. This is extracted from a thermal distribution truncated at $e_{\max} = 10^{-4}$ (blue, top), $e_{\max} = 10^{-3}$ (grey, middle), and $e_{\max} = 10^{-2}$ (red, bottom). Dashed horizontal lines mark the Hellinger distances values corresponding 1 and 5 σ -levels (cf. Table I).

(higher) SNR tend to have larger (smaller) values of d_H , corresponding to the regime where statistical systematic uncertainties dominate the error budget. This can also be seen by comparing the top and bottom panels of Fig. 1.

C. Marginalization with astrophysical models

The use of thermal distributions truncated at e_{\max} in the previous sections was arbitrary. We now present a more motivated strategy which makes direct use of state-of-the-art population-synthesis predictions. We interpret this as an “astrophysical marginalization” over the residual eccentricity: the back-propagated posteriors on the spin directions one infers are broader than one would obtain by naively assuming that binaries evolved on ideal quasi-circular orbits for their entire inspiral.

Eccentricity at merger is a distinct signature of binaries that formed in dynamical environments, notably dense stellar clusters. We use predictions obtained with RAPSTER [46] and CMC [45], which are two of the current state-of-the-art cluster codes in the field. These are compared against a population of BH binaries formed in isolation as predicted with the STARTRACK [44, 52] code. For binaries formed in clusters, we label sources as (i) “ejected” for BHs that merge outside of the cluster; (ii) “in-cluster” for BHs that merge inside the cluster following binary formation and (iii) “GW capture” which also merge inside the cluster but abruptly.

The RAPSTER population is generated based on the assumptions detailed in Sec. III. A of Ref. [65]. For STARTRACK, we use the population referred to as “default model” in Ref. [66]. Results from CMC are extracted from Fig. 1 of Ref. [21], which refers to detectable populations of sources at $f_{\text{ref}} = 10$ Hz. We eyeball their figure and consider skewed log-normal distributions with means of $10^{-6.8}$, $10^{-5.5}$, and $10^{-2.5}$, standard deviations of 10^{-1} , and skewness parameters of 9, 6, and 1 for the ejected, in-cluster and GW capture sub-channels, respectively. We weight each of these distributions as reported in Table II. For the RAPSTER and STARTRACK populations, eccentricity and spin distributions are provided at BH formation, which we forward-propagate to $f_{\text{ref}} = 10$ Hz as described in Sec. II A. For these two codes, we post-process information for the GW detectability by considering a single LIGO instrument and a SNR threshold of 8.

Signals are computed using the IMRPHEMOMX-PHM [55] waveform model and a noise power spectral density that is representative of the 4th observing run. This is consistent with the injections from Ref. [43] introduced in Sec. II C. We analytically marginalize over the extrinsic parameters [67, 68] as implemented in Ref. [69]. This results in a set of weights p_{det} for each source in our simulated populations, which is then normalized, i.e. we set $\sum_i p_{\text{det},i} = 1$. For RAPSTER, the fractional contributions of each of the three subchannels is reported in Table II.

Figure 3 shows the resulting residual eccentricities at $f_{\text{ref}} = 10$ Hz. The distributions predicted for each formation (sub)channel are quite distinct and differ by orders of magnitudes. Predictions from the two populations of dynamically assembled binaries are in broad agreement. With the notable exception of GW captures, residual eccentricities fall well below the current distinguishability

	Ejected	In-cluster	GW-capture
RAPSTER	0.71 (0.70)	0.20 (0.20)	0.09 (0.002)
CMC	0.70 (0.70)	0.20 (0.20)	0.10 (0.079)

TABLE II. Fractional contributions to the BH merger rate for the three sub-channels of the dynamical formation channel using predictions from RAPSTER and CMC. Numbers in parenthesis refer to sources with $e_{\text{res}} < e_{\text{thr}} = 0.05$.

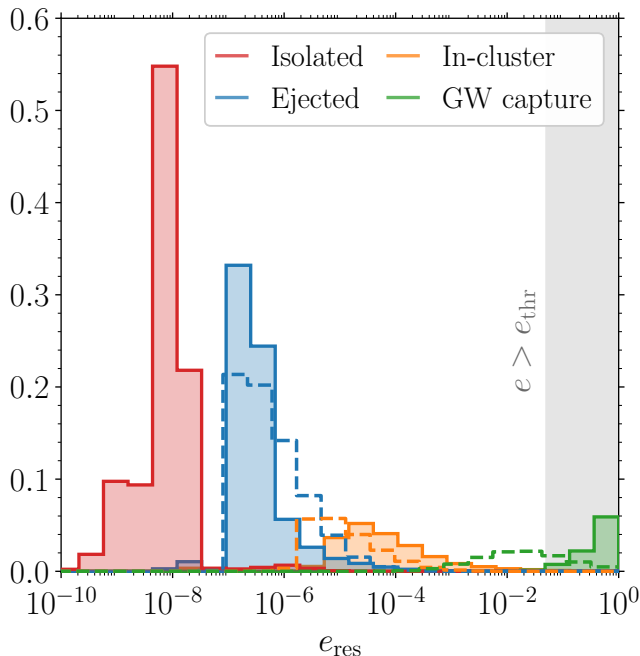


FIG. 3. Distributions of eccentricities at the reference frequency $f_{\text{ref}} = 10$ Hz for some representative astrophysical populations of BH binaries from stellar physics simulations. Distributions related to three sub-channels within the two dynamically formed populations are shown in blue for ejected binaries merging outside the cluster, orange for binaries merging inside the cluster, and green for binaries formed via GW captures. For these, solid and dashed histograms show predictions from the RAPSTER and CMC codes, respectively. The isolated-binary population from STARTRACK is shown in red. The grey area to the left mark systems with eccentricity larger than the resolvability threshold, here set to $e_{\text{thr}} = 0.05$. Binaries are weighted by their GW detectability and the resulting histograms are normalized to the cumulative detection probability, i.e. the sum of the bin heights for the isolated and dynamical channels is equal to 1. The contributions provided by each of the sub-channels is reported in Table II.

threshold $e_{\text{thr}} \simeq 0.05$ [42]. Even third-generation detectors, which might reach $e_{\text{thr}} \simeq 10^{-3}$ [70], will not be of much help here. In the following, we truncate the distributions of Fig. 3 to $e \leq e_{\text{thr}} \simeq 0.05$, which mimics a scenario where highly eccentric sources can be identified as such and thus do not pollute our inference of binaries that appear quasi-circular. Note that Fig. 3 is likely to over-estimate the importance of highly eccentric sources

because of the related difficulties with estimating GW detectability; this is partly motivates the difference between CMC and RAPSTER for the GW-capture subchannel.

Given these predictions, we perform the same operation discussed in Sec. III while drawing residual eccentricities from the distributions of Fig. 3. Figure 4 shows results for the same software injection considered in top panels of Fig. 1. We first propagate the GW posteriors forward from $f_{\text{ref}} = 20$ Hz (where the injections was performed) to 10 Hz (where the residual eccentricity is provided, see above). We then back-propagate spin directions to the joint large separation $a = 10^4 M$.

The results of Fig. 4 should be interpreted as our best estimate of the spin orientations at (or, more accurately, close to) BH formation given the detected GW data and *assuming* a specific formation pathway. Figure 4 shows the same trends highlighted in Sec. III A: distributions with the lowest (largest) residual eccentricity such as isolated binaries (GW captures) have back-propagated spin directions that are further (closer) to those at detection, and the main reason is that those binaries have a larger (lower) angular momentum. When considering contributions from all the dynamical sub-channels, our predictions sit close to the distributions for the ejected and in-cluster subchannels because those two classes dominate the dynamical formation merger rate, see Fig. 3 and Table II (recall that we are truncating the distribution at e_{thr} , which further diminishes the GW-capture contribution).

Crucially, the procedure we present heavily relies on the adopted astrophysical population, which is subject to significant uncertainties. Furthermore, our results do not capture correlations between the residual eccentricity and the other parameters (say the masses or the spins) of the back-propagated signal. While our results are indicative even for fixed populations, we ultimately envision this approach to be used in synchronicity with full GW population fits, the results of which can then be repurposed to shed light on individual detections, see e.g. Ref. [63].

IV. CONCLUSIONS

Some of the key observables in GW astronomy are time dependent, i.e. their values change, sometime significantly, as sources inspiral. Among these are the spin directions and the orbital eccentricity. Capturing their coupled evolution between BH formation and GW detection is important for an unbiased reconstruction of formation pathway of stellar-mass BH binaries. Current ground-based detectors are not able to distinguish eccentricities in BHs binaries which are $\lesssim 0.05$ at 10 Hz. Those sources are thus typically reported as compatible with binaries on quasi-circular orbits.

Eccentricity and spin inclinations are coupled [26] and, as illustrated in this paper, mismodeling in the former at detection translates into biased distributions of the latter at BH formation. Residual eccentricity is a systematic uncertainty for the spin directions, which should be con-

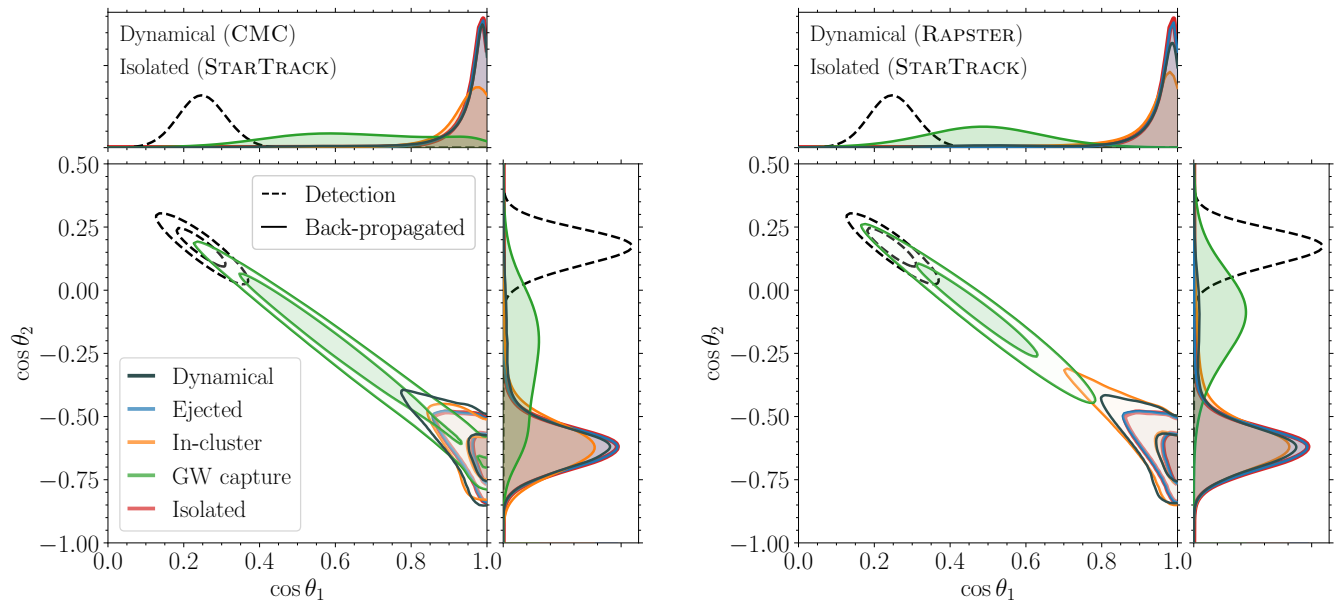


FIG. 4. Back-propagated posteriors of the spin directions assuming astrophysically motivated distributions of residual eccentricity. We consider the $\text{SNR} \sim 100$ synthetic signal `uni_88` from the dataset of Ref. [61] (cf. top panel of Fig. 1). Dashed curves show distributions at detection ($f_{\text{ref}} = 20$ Hz) while solid curves shows distribution at the common large separation ($a = 10^4 M$). Contours in the 2-dimensional distributions correspond to 50% and 90% credible intervals. The left (right) panel uses predictions for dynamically assembled BHs by the RAPSTER (CMC) code, see text for details. We show predictions from individual sub-channels (blue, orange, green) as well as a joint predictions that keeps into account the relative mixing fractions (dark grey). For reference both panels report results from an isolated-star distribution from STARTRACK (red), which are virtually indistinguishable from those obtained with the ejected subchannel (blue). An animated version of this figure is available at www.davidegerosa.com/spinprecession.

sidered in addition to the statistical uncertainty due to detector noise. In particular, our study illustrates that:

- (i) The systematic bias on the spin directions due to residual eccentricity increases with both the residual eccentricity itself as well as the amount of spin precession in the signals. This illustrates that this effect is indeed due to couplings between the precession and eccentricity sectors of the BH dynamics.
- (ii) For the events reported by LIGO/Virgo so far, the systematic uncertainty due to residual eccentricity is subdominant compared to the statistical uncertainty of the spin directions ($d_H \lesssim 0.01$).
- (iii) The situation is reversed for putative sources with $\text{SNR} \sim 100$ and precessing spins, which might present spin posteriors at BH formation that are essentially disjoint from those obtained assuming quasi-circular orbits ($d_H \sim 0.8$).

Residual eccentricity influences not only the spin predictions of individual events but also those of population-level analyses, which we plan to investigate in future work. Features in the inferred population of the BH spins are used to constrain specific mechanisms behind the assembly of BH binaries such as supernova kicks, tidal interactions, mass transfer, and even the symmetry of

the environment [10, 11, 14, 66, 71–77]. GW population fits that include spin directions are now performed after binaries have been back-propagated to past time infinity (i.e. $f_{\text{ref}} = 0$ Hz) assuming quasi-circular orbits [29, 30, 32]. The evolution of eccentric binaries to past time infinity is still an open problem because the commonly employed averaging techniques [26, 41] are expected to break down [28]. In this paper we sidestepped the issue by halting our evolution at a large but finite separation, $a = 10^4 M$. Extrapolating from what we presented here, we speculate that importance of the systematic bias due to residual eccentricity might increase if evolutions are extended to larger separations, though we stress this requires the development of an appropriate PN-evolution strategy in conjunction with a population fit in hierarchical Bayesian statistics.

Residual eccentricity might also impact archival searches of stellar-mass BH binaries in LISA data. It has been argued that ground-based detections of merging binaries might be used to “know where to look for,” thus digging deeper into the LISA noise and increasing the sensitivity of our searches [33, 35]. This paper shows that residual eccentricity is an important caveat to this statement; we will not really know where to look for. The uncertainty is further exacerbated by the known degeneracy between eccentricity and time to merger [78].

Still operating at the single-event level, we explored a

potential strategy to quantify the systematic error due to residual eccentricity when inferring the BH spin directions, which relies on pre-computed astrophysical distributions. While admittedly model-dependent, the procedure highlighted in this paper mitigates the eccentricity systematics by folding astrophysical modeling into the spin-orientation inference. The adopted astrophysical distribution of e_{res} is yet another systematic, but this is arguably better than blindly assuming $e_{\text{res}} = 0$ for all posterior samples of all the events as has been done so far.

ACKNOWLEDGMENTS

We thank Philippa Cole, Arianna Renzini, Ssohrab Borhanian, Nick Loutrel, Chris Moore, Ulrich Sperhake, Johan Samsing, and Fabio Antonini for discussions. G.F., D.G., and V.D.R. are supported by ERC

Starting Grant No. 945155–GWmining, Cariplo Foundation Grant No. 2021-0555, MUR PRIN Grant No. 2022-Z9X4XS, and the ICSC National Research Centre funded by NextGenerationEU. G.F. is supported by Sigma Xi Grant No. G20230315-4609 and an Erasmus+ scholarship. I.R.S. acknowledges support received from the Herchel Smith Postdoctoral Fellowship Fund. D.G. is supported by MSCA Fellowships No. 101064542–StochRewind and No. 101149270–ProtoBH. K.K. is supported by Onassis Foundation Scholarship No. FZT041-1/2023-2024, NSF Grants No. AST-2006538, PHY-2207502, PHY-090003 and PHY-20043, NASA Grants No. 20-LPS20-0011 and 21-ATP21-0010, John Templeton Foundation Grant No. 62840, Italian Ministry of Foreign Affairs and International Cooperation Grant No. PGR01167, and the Simons Foundation. A.O. is supported by the Foundation for Polish Science (FNP). Computational work was performed at CINECA with allocations through INFN and Bicocca.

-
- [1] B. P. Abbott *et al.*, *Phys. Rev. X* **9**, 031040 (2019), arXiv:1811.12907 [astro-ph.HE].
- [2] R. Abbott *et al.*, *Phys. Rev. X* **11**, 021053 (2021), arXiv:2010.14527 [gr-qc].
- [3] R. Abbott *et al.*, *Phys. Rev. D* **109**, 022001 (2024), arXiv:2108.01045 [gr-qc].
- [4] R. Abbott *et al.*, *Phys. Rev. X* **13**, 041039 (2023), arXiv:2111.03606 [gr-qc].
- [5] M. Mapelli, in *Handbook of Gravitational Wave Astronomy* (Springer, 2021) p. 16.
- [6] D. Gerosa and M. Fishbach, *Nat. Astron.* **5**, 749 (2021), arXiv:2105.03439 [astro-ph.HE].
- [7] I. Mandel and A. Farmer, *Phys. Rep.* **955**, 1 (2022), arXiv:1806.05820 [astro-ph.HE].
- [8] I. Mandel and F. S. Broekgaarden, *Living Rev. Relativ.* **25**, 1 (2022), arXiv:2107.14239 [astro-ph.HE].
- [9] M. Zevin, C. Pankow, C. L. Rodriguez, L. Sampson, E. Chase, V. Kalogera, and F. A. Rasio, *Astrophys. J.* **846**, 82 (2017), arXiv:1704.07379 [astro-ph.HE].
- [10] A. Q. Cheng, M. Zevin, and S. Vitale, *Astrophys. J.* **955**, 127 (2023), arXiv:2307.03129 [astro-ph.HE].
- [11] D. Gerosa, M. Kesden, E. Berti, R. O’Shaughnessy, and U. Sperhake, *Phys. Rev. D* **87**, 104028 (2013), arXiv:1302.4442 [gr-qc].
- [12] C. L. Rodriguez, M. Zevin, C. Pankow, V. Kalogera, and F. A. Rasio, *Astrophys. J. Lett.* **832**, L2 (2016), arXiv:1609.05916 [astro-ph.HE].
- [13] S. Vitale, R. Lynch, R. Sturani, and P. Graff, *Class. Quantum Grav.* **34**, 03LT01 (2017), arXiv:1503.04307 [gr-qc].
- [14] S. Stevenson, C. P. L. Berry, and I. Mandel, *Mon. Not. R. Astron. Soc.* **471**, 2801 (2017), arXiv:1703.06873 [astro-ph.HE].
- [15] D. Gerosa, E. Berti, R. O’Shaughnessy, K. Belczynski, M. Kesden, D. Wysocki, and W. Gladysz, *Phys. Rev. D* **98**, 084036 (2018), arXiv:1808.02491 [astro-ph.HE].
- [16] S. S. Bavera, T. Fragos, Y. Qin, E. Zapartas, C. J. Neijssel, I. Mandel, A. Batta, S. M. Gaebel, C. Kimball, and S. Stevenson, *Astron. Astrophys.* **635**, A97 (2020), arXiv:1906.12257 [astro-ph.HE].
- [17] A. Olejak and K. Belczynski, *Astrophys. J. Lett.* **921**, L2 (2021), arXiv:2109.06872 [astro-ph.HE].
- [18] S. Banerjee, A. Olejak, and K. Belczynski, *Astrophys. J.* **953**, 80 (2023), arXiv:2302.10851 [astro-ph.HE].
- [19] J. Samsing, M. MacLeod, and E. Ramirez-Ruiz, *Astrophys. J.* **784**, 71 (2014), arXiv:1308.2964 [astro-ph.HE].
- [20] J. Samsing, *Phys. Rev. D* **97**, 103014 (2018), arXiv:1711.07452 [astro-ph.HE].
- [21] M. Zevin, I. M. Romero-Shaw, K. Kremer, E. Thrane, and P. D. Lasky, *Astrophys. J. Lett.* **921**, L43 (2021), arXiv:2106.09042 [astro-ph.HE].
- [22] T. A. Apostolatos, C. Cutler, G. J. Sussman, and K. S. Thorne, *Phys. Rev. D* **49**, 6274 (1994).
- [23] L. E. Kidder, *Phys. Rev. D* **52**, 821 (1995), arXiv:gr-qc/9506022 [gr-qc].
- [24] I. M. Romero-Shaw, P. D. Lasky, and E. Thrane, *Mon. Not. R. Astron. Soc.* **490**, 5210 (2019), arXiv:1909.05466 [astro-ph.HE].
- [25] I. M. Romero-Shaw, D. Gerosa, and N. Loutrel, *Mon. Not. R. Astron. Soc.* **519**, 5352 (2023), arXiv:2211.07528 [astro-ph.HE].
- [26] G. Fumagalli and D. Gerosa, *Phys. Rev. D* **108**, 124055 (2023), arXiv:2310.16893 [gr-qc].
- [27] D. Gerosa, M. Kesden, U. Sperhake, E. Berti, and R. O’Shaughnessy, *Phys. Rev. D* **92**, 064016 (2015), arXiv:1506.03492 [gr-qc].
- [28] D. Gerosa, G. Fumagalli, M. Mould, G. Cavallotto, D. P. Monroy, D. Gangardt, and V. De Renzi, *Phys. Rev. D* **108**, 024042 (2023), arXiv:2304.04801 [gr-qc].
- [29] M. Mould and D. Gerosa, *Phys. Rev. D* **105**, 024076 (2022), arXiv:2110.05507 [astro-ph.HE].
- [30] N. K. Johnson-McDaniel, S. Kulkarni, and A. Gupta, *Phys. Rev. D* **106**, 023001 (2022), arXiv:2107.11902 [astro-ph.HE].
- [31] S. Kulkarni, N. K. Johnson-McDaniel, K. S. Phukon, N. V. Krishnendu, and A. Gupta, *Phys. Rev. D* **109**, 043002 (2024), arXiv:2308.05098 [astro-ph.HE].
- [32] R. Abbott *et al.*, *Phys. Rev. X* **13**, 011048 (2023), arXiv:2111.03634 [astro-ph.HE].

- [33] K. W. K. Wong, E. D. Kovetz, C. Cutler, and E. Berti, *Phys. Rev. Lett.* **121**, 251102 (2018), arXiv:1808.08247 [astro-ph.HE].
- [34] D. Gerosa, S. Ma, K. W. K. Wong, E. Berti, R. O’Shaughnessy, Y. Chen, and K. Belczynski, *Phys. Rev. D* **99**, 103004 (2019), arXiv:1902.00021 [astro-ph.HE].
- [35] B. Ewing, S. Sachdev, S. Borhanian, and B. S. Sathyaprakash, *Phys. Rev. D* **103**, 023025 (2021), arXiv:2011.03036 [gr-qc].
- [36] A. Toubiana, S. Babak, S. Marsat, and S. Ossokine, *Phys. Rev. D* **106**, 104034 (2022), arXiv:2206.12439 [gr-qc].
- [37] B. P. Abbott *et al.*, *Astrophys. J.* **883**, 149 (2019).
- [38] A. G. Abac *et al.*, (2023), arXiv:2308.03822 [astro-ph.HE].
- [39] I. Romero-Shaw, P. D. Lasky, and E. Thrane, *Astrophys. J.* **940**, 171 (2022), arXiv:2206.14695 [astro-ph.HE].
- [40] N. Gupte, A. Ramos-Buades, A. Buonanno, J. Gair, M. C. Miller, M. Dax, S. R. Green, M. Pürrer, J. Wildberger, J. Macke, and B. Schölkopf, (2024), arXiv:2404.14286 [gr-qc].
- [41] P. C. Peters, *Phys. Rev.* **136**, 1224 (1964).
- [42] M. E. Lower, E. Thrane, P. D. Lasky, and R. Smith, *Phys. Rev. D* **98**, 083028 (2018), arXiv:1806.05350 [astro-ph.HE].
- [43] V. De Renzi, D. Gerosa, G. Pratten, P. Schmidt, and M. Mould, *Phys. Rev. D* **106**, 084040 (2022), arXiv:2207.00030 [gr-qc].
- [44] A. Olejak, C. L. Fryer, K. Belczynski, and V. Baibhav, *Mon. Not. R. Astron. Soc.* **516**, 2252 (2022), arXiv:2204.09061 [astro-ph.HE].
- [45] K. Kremer, C. S. Ye, N. Z. Rui, N. C. Weatherford, S. Chatterjee, G. Fragione, C. L. Rodriguez, M. Spera, and F. A. Rasio, *Astrophys. J. Supp. S.* **247**, 48 (2020), arXiv:1911.00018 [astro-ph.HE].
- [46] K. Kritos, V. Stokov, V. Baibhav, and E. Berti, (2022), arXiv:2210.10055 [astro-ph.HE].
- [47] É. Racine, *Phys. Rev. D* **78**, 044021 (2008), arXiv:0803.1820 [gr-qc].
- [48] P. Schmidt, F. Ohme, and M. Hannam, *Phys. Rev. D* **91**, 024043 (2015), arXiv:1408.1810 [gr-qc].
- [49] D. Gerosa, M. Mould, D. Gangardt, P. Schmidt, G. Pratten, and L. M. Thomas, *Phys. Rev. D* **103**, 064067 (2021), arXiv:2011.11948 [gr-qc].
- [50] M. Kesden, D. Gerosa, R. O’Shaughnessy, E. Berti, and U. Sperhake, *Phys. Rev. Lett.* **114**, 081103 (2015), arXiv:1411.0674 [gr-qc].
- [51] I. Romero-Shaw, P. D. Lasky, and E. Thrane, *Astrophys. J. Lett.* **921**, L31 (2021), arXiv:2108.01284 [astro-ph.HE].
- [52] K. Belczynski, J. Klencki, C. E. Fields, A. Olejak, E. Berti, G. Meynet, C. L. Fryer, D. E. Holz, R. O’Shaughnessy, D. A. Brown, T. Bulik, S. C. Leung, K. Nomoto, P. Madau, R. Hirschi, E. Kaiser, S. Jones, S. Mondal, M. Chruslinska, P. Drozda, D. Gerosa, Z. Doctor, M. Giersz, S. Ekstrom, C. Georgy, A. Askar, V. Baibhav, D. Wysocki, T. Natan, W. M. Farr, G. Wiktorowicz, M. Coleman Miller, B. Farr, and J. P. Lasota, *Astron. Astrophys.* **636**, A104 (2020), arXiv:1706.07053 [astro-ph.HE].
- [53] M. Mapelli, *Frontiers in Astronomy and Space Sciences* **7**, 38 (2020), arXiv:2105.12455 [astro-ph.HE].
- [54] F. Antonini and M. Gieles, *Mon. Not. R. Astron. Soc.* **492**, 2936 (2020), arXiv:1906.11855 [astro-ph.HE].
- [55] G. Pratten, C. García-Quirós, M. Colleoni, A. Ramos-Buades, H. Estellés, M. Mateu-Lucena, R. Jaume, M. Haney, D. Keitel, J. E. Thompson, and S. Husa, *Phys. Rev. D* **103**, 104056 (2021), arXiv:2004.06503 [gr-qc].
- [56] S. Ossokine, A. Buonanno, S. Marsat, R. Cotesta, S. Babak, T. Dietrich, R. Haas, I. Hinder, H. P. Pfeiffer, M. Pürrer, C. J. Woodford, M. Boyle, L. E. Kidder, M. A. Scheel, and B. Szilágyi, *Phys. Rev. D* **102**, 044055 (2020), arXiv:2004.09442 [gr-qc].
- [57] V. Varma, S. E. Field, M. A. Scheel, J. Blackman, D. Gerosa, L. C. Stein, L. E. Kidder, and H. P. Pfeiffer, *Phys. Rev. Res.* **1**, 033015 (2019), arXiv:1905.09300 [gr-qc].
- [58] M. Hannam, C. Hoy, J. E. Thompson, S. Fairhurst, V. Raymond, *et al.*, *Nature* **610**, 652 (2022), arXiv:2112.11300 [gr-qc].
- [59] V. Varma, S. Biscoveanu, T. Islam, F. H. Shaik, C.-J. Haster, M. Isi, W. M. Farr, S. E. Field, and S. Vitale, *Phys. Rev. Lett.* **128**, 191102 (2022), arXiv:2201.01302 [astro-ph.HE].
- [60] E. Payne, S. Hourihane, J. Golomb, R. Udall, D. Davis, and K. Chatziioannou, *Phys. Rev. D* **106**, 104017 (2022), arXiv:2206.11932 [gr-qc].
- [61] V. De Renzi and D. Gerosa, github.com/ViolaDeRenzi/twoprecessingspins, doi.org/10.5281/zenodo.6777952 (2022).
- [62] J. Chung, P. Kannappan, C. T. Ng, and P. Sahoo, *J. Math. Anal. Appl.* **138**, 280 (1989).
- [63] C. J. Moore and D. Gerosa, *Phys. Rev. D* **104**, 083008 (2021), arXiv:2108.02462 [gr-qc].
- [64] A. Klein, (2021), arXiv:2106.10291 [gr-qc].
- [65] S. Yi, A. Kuntz, E. Barausse, E. Berti, M. Ho-Yeuk Cheung, K. Kritos, and A. Maselli, (2024), arXiv:2403.09767 [gr-qc].
- [66] A. Olejak, J. Klencki, X.-T. Xu, C. Wang, K. Belczynski, and J.-P. Lasota, (2024), arXiv:2404.12426 [astro-ph.HE].
- [67] L. S. Finn and D. F. Chernoff, *Phys. Rev. D* **47**, 2198 (1993), arXiv:gr-qc/9301003 [gr-qc].
- [68] D. Gerosa and M. Bellotti, *Class. Quantum Grav.* **41**, 125002 (2024), arXiv:2404.16930 [astro-ph.HE].
- [69] D. Gerosa, github.com/dgerosa/gwdet, doi.org/10.5281/zenodo.889966 (2017).
- [70] P. Saini, *Mon. Not. R. Astron. Soc.* **528**, 833 (2024), arXiv:2308.07565 [astro-ph.HE].
- [71] J. Stegmann and F. Antonini, *Phys. Rev. D* **103**, 063007 (2021), arXiv:2012.06329 [astro-ph.HE].
- [72] N. Steinle and M. Kesden, *Phys. Rev. D* **103**, 063032 (2021), arXiv:2010.00078 [astro-ph.HE].
- [73] B. McKernan, K. E. S. Ford, T. Callister, W. M. Farr, R. O’Shaughnessy, R. Smith, E. Thrane, and A. Vajpeyi, *Mon. Not. R. Astron. Soc.* **514**, 3886 (2022), arXiv:2107.07551 [astro-ph.HE].
- [74] T. M. Tauris, *Astrophys. J.* **938**, 66 (2022), arXiv:2205.02541 [astro-ph.HE].
- [75] M. Mould, D. Gerosa, F. S. Broekgaarden, and N. Steinle, *Mon. Not. R. Astron. Soc.* **517**, 2738 (2022), arXiv:2205.12329 [astro-ph.HE].
- [76] A. Santini, D. Gerosa, R. Cotesta, and E. Berti, *Phys. Rev. D* **108**, 083033 (2023), arXiv:2308.12998 [astro-ph.HE].
- [77] C. Adamcewicz, S. Galadage, P. D. Lasky, and E. Thrane, *Astrophys. J. Lett.* **964**, L6 (2024), arXiv:2311.05182 [astro-ph.HE].
- [78] R. Busicchio, A. Klein, E. Roebber, C. J. Moore, D. Gerosa, E. Finch, and A. Vecchio, *Phys. Rev. D* **104**, 044065 (2021), arXiv:2106.05259 [astro-ph.HE].